Journal of Sound and Vibration (1997) **202**(1), 55–66

EXPERIMENTAL MEASUREMENT OF PRECISION BEARING DYNAMIC STIFFNESS

E. R. Marsh and D. S. Yantek

Department of Mechanical Engineering, The Pennsylvania State University, University Park, PA 16802, *U.S.A.*

(*Received* 19 *February* 1996, *and in final form* 9 *September* 1996)

Static stiffness measurement of precision bearing components by influence coefficients is complicated by the task of loading and measuring the baseline test fixture stiffness before including the bearing components. Furthermore, as the displacement of the bearing system is measured for various load conditions, the stiffness of high quality bearings may be difficult to distinguish from the test fixture stiffness. The common occurrence of inaccurate stiffness measurements has motivated this investigation of an experimental method based on frequency response function measurements. In this work the traditional static measurement that requires careful attachment and modelling of the test fixture to "ground" is abandoned and replaced by dynamic measurements taken from a test fixture with free boundary conditions. A complete dynamic characterization of the test fixture is shown to be unnecessary; the only measurements required are the frequency response functions at the points of attachment to the bearing components. An investigation into the effects of common measurement errors such as sensor calibration and location is also included, with an example of the proposed method.

1. INTRODUCTION

Several recent works have made significant contributions to the experimental measurement of rotary and linear bearings. The requirements of the rotating equipment and precision engineering community have motivated important work in the area of in-service measurement of bearing parameters. A summary paper by Stone [1] reviews three research efforts to measure rolling element bearing stiffness under various amounts of preload, speed and lubrication. Walford and Stone [2, 3] use a two-degree-of-freedom mathematical model to extract a representative stiffness value. The simple model used in these works provides a means of comparing the stiffness of the bearing system under a variety of operating and design parameters. Kraus *et al*. [4] provide an update to these earlier works by Walford and Stone using the more modern experimental modal analysis equipment and techniques available today. They retain the use of the two-degree-of-freedom model.

Other works add analyses capable of estimating the stiffness of a bearing under operating conditions without the requirement that a known input force be used to excite the system. Tiwari and Vyas [5] offer a means of estimating the bearing stiffness without explicit force measurements provided that the system may be assumed to be perfectly balanced. They assume the bearing system excitation results from random imperfections in the bearing surfaces and assembly. Their analysis uses a stochastic characterization of the bearing excitation in conjunction with a single-degree-of-freedom model to estimate a representative stiffness.

The work described in this paper develops an alternative means of evaluating the stiffness of bearing components. The formulation of the stiffness estimation problem and the

0022–460X/97/160055 + 12 $25.00/0/sv960793

accompanying experimental technique requires the use of known excitation forces (e.g., measured impact hammer blows) and the resulting responses (e.g., as measured by accelerometers). As with any experimental technique, the proposed stiffness estimation technique involves several issues that must be addressed to ensure confidence in the method. The precise location of the input and output measurements, sensor calibration, and the number of measurements are all critical to the method's success. The work that follows investigates these issues and provides an example of the successful implementation of the method.

2. PROBLEM FORMULATION

High bearing pre-loads and moderate loading allow the stiffness estimation problem to be considered from the framework of any of the three traditional linear system model formulations: spatial ($\mathbf{M}\ddot{x} + \mathbf{C}\dot{x} + \mathbf{K}x = f$), frequency ($\mathbf{X} = \mathbf{H}(\omega)\mathbf{F}$) and modal ($\mathbf{U}^{\mathrm{T}}\mathbf{M}\mathbf{U}\ddot{\eta} + \mathbf{U}^{\mathrm{T}}\mathbf{C}\mathbf{U}\dot{\eta} + \mathbf{U}^{\mathrm{T}}\mathbf{K}\mathbf{U}\eta = \mathbf{U}^{T}f$). The works cited above use a modal model formulation to extract a representative bearing stiffness. In this approach, a frequency domain model is used to obtain an estimate of bearing stiffness, a spatial domain quantity. Lee and Dobson review the challenging problem of calculating mass, stiffness, and damping parameters from a frequency domain model [6, 7]. Knowledge of the location of the bearing components in the test fixture simplifies the formulation.

The development of the stiffness estimation method proceeds by considering, without loss of generality, the estimation of a single spring stiffness (the bearing) from a system of two Euler beams (the test fixture). The geometry of the system that will be used to develop the stiffness estimation procedure is outlined in Figure 1.

The well known dynamics of the Euler beams are assumed to behave linearly and are modelled with a discrete representation of arbitrary order N. The upper and lower cantilever beams serve as the two halves of the test fixture that constrain the bearing. In a machine tool spindle, the two halves would be the stator and rotor. In a machine axis, the carriage and slideways envelop the bearings. The governing differential equations of motion of the test fixture halves may be assembled in block matrix form. The halves of the test fixture model are denoted by the subscripts 1 and 2. Note that the bearing matrices $\mathbf{M}_B$ and $\mathbf{K}_B$ overlap with the structure's mass and stiffness matrices. This provides the mathematical coupling of the physical connection:

$$\left(\begin{bmatrix}\mathbf{M}_1 & \\ & \mathbf{M}_2\end{bmatrix} + \begin{bmatrix} & \\ & \mathbf{M}_B\end{bmatrix}\right)\begin{Bmatrix}\ddot{x}_1\\ \ddot{x}_2\end{Bmatrix} + \left(\begin{bmatrix}\mathbf{K}_1 & \\ & \mathbf{K}_2\end{bmatrix} + \begin{bmatrix} & \\ & \mathbf{K}_B\end{bmatrix}\right)\begin{Bmatrix}x_1\\ x_2\end{Bmatrix} = \begin{Bmatrix}f_1\\ f_2\end{Bmatrix}, \tag{1}$$

where $\mathbf{M}_1$ is the mass matrix of the first half of the test fixture ($m \times m$), $\mathbf{M}_2$ is the mass matrix of the second half ($n \times n$), $\mathbf{M}_B$ is the mass matrix of the bearing assembly ($p \times p$),

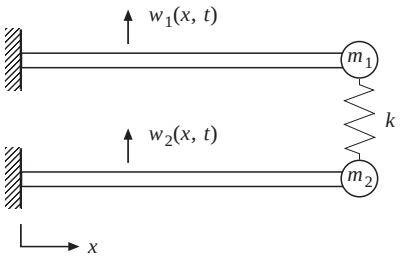

Figure 1. Two cantilever beams (the bearing test fixture) with a bearing modelled with lumped masses m_1, and m_2 and stiffness k.

$\mathbf{K}_1$ is the stiffness matrix of the first half of the test fixture ($m \times m$), $\mathbf{K}_2$ is the stiffness matrix of the second half ($n \times n$), $\mathbf{K}_B$ is the stiffness matrix of the bearing assembly ($p \times p$), x_1 is the displacement vector of the first half of the test fixture ($m \times 1$), x_2 is the displacement vector of the second half ($n \times 1$), f_1 is the forcing function on the first half of the test fixture ($m \times 1$), f_2 is the forcing function on the second half ($n \times 1$), $N = m + n$.

The bearings connect the two halves of the test fixture, resulting in coupled mass and stiffness matrices for the fully assembled structure. For convenience, the uncoupled stiffness and mass matrix of the test fixture are called $\mathbf{K}_0$ and $\mathbf{M}_0$ and the coupled matrices of the total system are called $\mathbf{K}_{total}$ and $\mathbf{M}_{total}$. The matrices $\mathbf{K}_B$ and $\mathbf{M}_b$ contain zero entries except at the degrees of freedom corresponding to bearing connection points:

$$\mathbf{K}_{total} = \mathbf{K}_0 + \mathbf{K}_b, \qquad \mathbf{M}_{total} = \mathbf{M}_0 + \mathbf{M}_b, \tag{2}$$

where

$$\mathbf{K}_0 = \begin{bmatrix} \mathbf{K}_1 & \\ & \mathbf{K}_2 \end{bmatrix}, \qquad \mathbf{K}_b = \begin{bmatrix} & & \\ & \mathbf{K}_B & \\ & & \end{bmatrix}, \qquad \mathbf{M}_0 = \begin{bmatrix} \mathbf{M}_1 & \\ & \mathbf{M}_2 \end{bmatrix}, \qquad \mathbf{M}_b = \begin{bmatrix} & & \\ & \mathbf{M}_B & \\ & & \end{bmatrix}.$$

The Fourier transform of the governing equations yields the classical frequency domain impedance matrices of linear multi-degree-of-freedom systems. The impedance matrix will be required for the system with and without the bearing in place:

$$\mathbf{Z}(\omega)\mathbf{X}(\omega) = \mathbf{F}(\omega), \qquad \mathbf{Z}_0(\omega)\mathbf{X}_0(\omega) = \mathbf{F}_0(\omega), \tag{3}$$

where

$$\mathbf{Z}(\omega) = -\omega^2\mathbf{M}_{total} + \mathbf{K}_{total}, \qquad \mathbf{Z}_0(\omega) = -\omega^2\mathbf{M}_0 + \mathbf{K}_0.$$

In equation (4), the difference of the two impedance matrices provides the mass and stiffness of the bearing components, in this case a single spring. Experience with the proposed method shows that although the bearing mass may be estimated alongside the bearing stiffness, a more accurate stiffness estimate may be obtained by using a measured value of the bearing mass. In practice, many types of bearings may be dissembled without removal from the test fixture. In this desirable case, the mass of the bearing is not needed explicitly because the component mass included in $\mathbf{M}_b$ will be present in both $\mathbf{Z}$ and $\mathbf{Z}_0$. The quantity of interest, $\mathbf{K}_B$, would then be available if the $2p^2$ dynamic impedance measurements could be taken (p^2 when the bearing is connected and p^2 when unconnected), recalling that p is the number of connection points in the bearings:

$$\mathbf{Z} - \mathbf{Z}_0 = \Delta\mathbf{Z} = \mathbf{K}_b, \qquad \begin{bmatrix} & & \\ & \mathbf{K}_B & \\ & & \end{bmatrix} = \Delta\mathbf{Z}, \tag{4a}$$

where $\mathbf{K}_B$ is the bearing impedance matrix.

As a second alternative, if the mass of the bearing $\mathbf{M}_B$ may be measured directly, the bearing is removed during measurement of the unconnected test fixture ($\mathbf{Z}_0$) and the change in impedance with the connection of the bearing includes the known bearing mass:

$$\mathbf{Z} - \mathbf{Z}_0 = \Delta\mathbf{Z} = -\omega^2\mathbf{M}_b + \mathbf{K}_b, \qquad \begin{bmatrix} & & \\ & \mathbf{K}_B & \\ & & \end{bmatrix} = \Delta\mathbf{Z} + \omega^2\begin{bmatrix} & & \\ & \mathbf{M}_B & \\ & & \end{bmatrix}. \tag{4b}$$

Finally, the bearing mass can be treated as an unknown to be estimated alongside the stiffness of the bearing components. This case is treated in the same manner. For clarity,

and without loss of generality, the mass is assumed to be unchanged in the measurements of the connected and unconnected test fixture (equation (4a)).

The matrix representation of the change in bearing system impedance highlights the difficulty of modern static measurement techniques because of the finite stiffness (non-zero compliance) of the test fixture. Even with static measurements, the effect of the test fixture stiffness must be included, but may be difficult to measure independently of the bearings. For example, the measurement of a machine tool slideway stiffness by traditional influence coefficients may be impossible for lack of a satisfactory method of connecting the test fixture components to ground when disconnected from the bearings.

Investigation of reliable experimental techniques to capture the stiffness of both test fixture and bearing components reveals the suitability of the classical linear input–output frequency response function (FRF). These dynamic measurements may be taken with arbitrary boundary conditions and are therefore used to estimate the stiffness from FRF measurements taken at discrete locations on the test fixture. Clearly, it is impractical to measure the arbitrarily numerous N^2 FRF's required to complete the matrix inverse of the FRF matrix $\mathbf{Z} = \mathbf{H}^{-1}$. Instead, a portion of the total $\mathbf{H}$ matrix is selected to find $\mathbf{K}_B$. A transformation matrix $\mathbf{T}$ reduces the total number of required measurements to a much smaller set of l^2 measurements. Equation (4a) is pre-multiplied by $\mathbf{T}$ and post-multiplied by the transpose of $\mathbf{T}$ to obtain equation (5):

$$\mathbf{T}\Delta\mathbf{Z}\mathbf{T}^{\mathrm{T}} = (\mathbf{T}\mathbf{H}\mathbf{T}^{\mathrm{T}})^{-1} - (\mathbf{T}\mathbf{H}_0\mathbf{T}^{\mathrm{T}})^{-1}, \tag{5}$$

where $\mathbf{T}\Delta\mathbf{Z}\mathbf{T}^{\mathrm{T}}$ is the bearing impedence matrix evaluated at measurement locations ($l \times l$), $\mathbf{T}\mathbf{H}\mathbf{T}^{\mathrm{T}}$ is the frequency response matrix evaluated at measurement locations ($l \times l$), $\mathbf{T}$ is the transformation matrix that picks out measurement locations ($l \times N$), $\mathbf{H} = \mathbf{Z}^{-1}$($N \times N$ FRF matrix) and $\mathbf{H}_0 = \mathbf{Z}_0^{-1}$($N \times N$ FRF matrix).

The next section provides an analysis indicating which of the many FRF's are required to complete the estimation (remembering that N may be arbitrarily large). This will allow the accurate construction of the $\mathbf{T}$ matrix by specifying the minimum number of appropriate measurements.

3. MINIMUM NUMBER OF MEASUREMENTS TO ESTIMATE STIFFNESS

To determine the minimum number of experimental measurements required to estimate the stiffness of a bearing, the dimension and contents of the transformation matrix $\mathbf{T}$ are simultaneously found. Without loss of generality, a single bearing acting in one direction in the test fixture is considered (as shown in Figure 1). The mass of the bearing is assumed to be known. Energy dissipation in the bearings, which may be significant in precision bearings when compared to the elastic test fixture, may be included using the hysteritic (structural) damping model, but is omitted for clarity.

The bearing stiffness of the spring of Figure 1 may be represented as

$$\mathbf{K}_B = k\boldsymbol{\varepsilon}\boldsymbol{\varepsilon}^{\mathrm{T}}, \tag{6}$$

where k is the bearing stiffness (scalar), $\boldsymbol{\varepsilon}_i = [\,\ldots\,1\;\;0\,\ldots\,]^{\mathrm{T}}$ is a vector of zeros with a 1 at one bearing connection location (DOFi), $\boldsymbol{\varepsilon}_j = [\,\ldots\,0\;\;1\,\ldots\,]^{\mathrm{T}}$ is a vector of zeros with a 1 at the other bearing connection location (DOFj), and $\boldsymbol{\varepsilon} = \boldsymbol{\varepsilon}_i - \boldsymbol{\varepsilon}_j$.

Upon substitution of the bearing stiffness matrix, the equation for the bearing stiffness (equation (5)) takes on a special form that may be manipulated with the Sherman Morrison equation:

$$\mathbf{T}\Delta\mathbf{Z}\mathbf{T}^{\mathrm{T}} = (\mathbf{T}(\mathbf{Z}_0 + k\boldsymbol{\varepsilon}\boldsymbol{\varepsilon}^{\mathrm{T}})^{-1}\mathbf{T}^{\mathrm{T}})^{-1} - (\mathbf{T}\mathbf{Z}_0^{-1}\mathbf{T}^{\mathrm{T}})^{-1}. \tag{7}$$

By the Sherman Morrison equation, a matrix $\mathbf{A}$ and its inverse can be used to find the inverse of a matrix $\mathbf{B}$ if $\mathbf{B}$ is equal to the sum of $\mathbf{A}$ and a column–row matrix vw^T:

$$\text{If } B = A - vw^{\mathrm{T}}, \text{ then } B^{-1} = A^{-1} - \frac{1}{w^{\mathrm{T}}A^{-1}v - 1} A^{-1}vw^{\mathrm{T}}A^{-1}. \tag{8}$$

By applying the Sherman Morrison equation to equation (7) and invoking the symmetry of the impedance matrix $\mathbf{Z}_0$, the inner inverse in the first term of the right side is eliminated:

$$\mathbf{T}\Delta\mathbf{Z}\mathbf{T}^{\mathrm{T}} = (\mathbf{T}\mathbf{Z}_0^{-1}\mathbf{T}^{\mathrm{T}} - c(\mathbf{T}\mathbf{Z}_0^{-1}\varepsilon)(\mathbf{T}\mathbf{Z}_0^{-1}\varepsilon)^{\mathrm{T}})^{-1} - (\mathbf{T}\mathbf{Z}_0^{-1}\mathbf{T}^{\mathrm{T}})^{-1}, \tag{9}$$

where

$$c = \frac{k}{k\boldsymbol{\varepsilon}^{\mathrm{T}}\mathbf{Z}_0^{-1}\boldsymbol{\varepsilon} + 1}$$

The new bearing stiffness equation (equation (9)) again fits the form of Sherman Morrison equation (equation (8)), so it is invoked a second time to eliminate the first inverse term.

$$\mathbf{T}\Delta\mathbf{Z}\mathbf{T}^{\mathrm{T}} = (\mathbf{T}\mathbf{Z}_0^{-1}\mathbf{T}^{\mathrm{T}})^{-1} - cd(\mathbf{T}\mathbf{Z}_0^{-1}\mathbf{T}^{\mathrm{T}})^{-1}(\mathbf{T}\mathbf{Z}_0^{-1}\boldsymbol{\varepsilon})\mathbf{T}\mathbf{Z}_0^{-1}\boldsymbol{\varepsilon})^{\mathrm{T}}(\mathbf{T}\mathbf{Z}_0^{-1}\mathbf{T}^{\mathrm{T}})^{-1} - (\mathbf{T}\mathbf{Z}_0^{-1}\mathbf{T}^{\mathrm{T}})^{-1}, \tag{10}$$

where

$$d = \frac{1}{c(\mathbf{T}\mathbf{Z}_0^{-1}\boldsymbol{\varepsilon})^{\mathrm{T}}(\mathbf{T}\mathbf{Z}_0^{-1}\mathbf{T}^{\mathrm{T}})^{-1}(\mathbf{T}\mathbf{Z}_0^{-1}\boldsymbol{\varepsilon}) - 1}.$$

Upon simplification, an equation for the impedance of the bearing is found. This equation is a function of the reduced impedance matrix ($\mathbf{T}\mathbf{Z}_0\mathbf{T}^{\mathrm{T}}$) of the full impedance matrix ($\mathbf{Z}_0$):

$$\mathbf{T}\Delta\mathbf{Z}\mathbf{T}^{\mathrm{T}} = k\frac{(\mathbf{T}\mathbf{Z}_0^{-1}\mathbf{T}^{\mathrm{T}})^{-1}(\mathbf{T}\mathbf{Z}_0^{-1}\boldsymbol{\varepsilon})(\mathbf{T}\mathbf{Z}_0^{-1}\boldsymbol{\varepsilon})^{\mathrm{T}}(\mathbf{T}\mathbf{Z}_0^{-1}\mathbf{T}^{\mathrm{T}})^{-1}}{1 - k[(\mathbf{T}\mathbf{Z}_0^{-1}\boldsymbol{\varepsilon})^{\mathrm{T}}(\mathbf{T}\mathbf{Z}_0^{-1}\mathbf{T}^{\mathrm{T}})^{-1}(\mathbf{T}\mathbf{Z}_0^{-1}\boldsymbol{\varepsilon}) - \boldsymbol{\varepsilon}^{\mathrm{T}}\mathbf{Z}_0^{-1}\boldsymbol{\varepsilon}]}, \tag{11}$$

where

$$\mathbf{T} = \begin{bmatrix} \boldsymbol{\varepsilon}_a^{\mathrm{T}} \\ \boldsymbol{\varepsilon}_b^{\mathrm{T}} \\ \vdots \end{bmatrix},$$

$$\mathbf{T}\mathbf{Z}_0^{-1}\mathbf{T}^{\mathrm{T}} = \begin{bmatrix} \boldsymbol{\varepsilon}_a^{\mathrm{T}} \\ \boldsymbol{\varepsilon}_b^{\mathrm{T}} \\ \vdots \end{bmatrix}\begin{bmatrix} (Z_0^{-1})_{11} & \cdots & (Z_0^{-1})_{1N} \\ \vdots & \ddots & \\ (Z_0^{-1})_{N1} & & (Z_0^{-1})_{NN} \end{bmatrix}[\boldsymbol{\varepsilon}_a \quad \boldsymbol{\varepsilon}_b \quad \cdots] = \begin{bmatrix} (Z_0^{-1})_{aa} & (Z_0^{-1})_{ab} & \\ (Z_0^{-1})_{ba} & (Z_0^{-1})_{bb} & \\ & & \ddots \end{bmatrix},$$

$$\mathbf{T}\mathbf{Z}_0^{-1}\boldsymbol{\varepsilon} = \begin{bmatrix} \boldsymbol{\varepsilon}_a^{\mathrm{T}} \\ \boldsymbol{\varepsilon}_b^{\mathrm{T}} \\ \vdots \end{bmatrix}\begin{bmatrix} (Z_0^{-1})_{11} & \cdots & (Z_0^{-1})_{1N} \\ \vdots & \ddots & \\ (Z_0^{-1})_{N1} & & (Z_0^{-1})_{NN} \end{bmatrix}\{\boldsymbol{\varepsilon}_i - \boldsymbol{\varepsilon}_j\} = \begin{Bmatrix} (Z_0^{-1})_{ai} - (Z_0^{-1})_{aj} \\ (Z_0^{-1})_{bi} - (Z_0^{-1})_{bj} \\ \vdots \end{Bmatrix},$$

$$\boldsymbol{\varepsilon}^{\mathrm{T}}\mathbf{Z}_0^{-1} = \{\boldsymbol{\varepsilon}_i^{\mathrm{T}} - \boldsymbol{\varepsilon}_j^{\mathrm{T}}\}\begin{bmatrix} (Z_0^{-1})_{11} & \cdots & (Z_0^{-1})_{1N} \\ \vdots & \ddots & \\ (Z_0^{-1})_{N1} & & (Z_0^{-1})_{NN} \end{bmatrix}\{\boldsymbol{\varepsilon}_i - \boldsymbol{\varepsilon}_j\} = (Z_0^{-1})_{ii} - 2(Z_0^{-1})_{ij} + (Z_0^{-1})_{jj}.$$

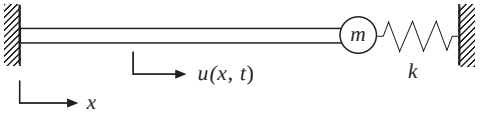

Figure 2. A rod in longitudinal deformation (the bearing test fixture) with attached spring and mass (the bearing).

Investigation of the bearing impedance equation (equation (11)) reveals that the transformation matrix **T** need only contain the vectors $\boldsymbol{\varepsilon}_i$ and $\boldsymbol{\varepsilon}_j$. Then, the denominator of equation (11) simplifies to unity because the bracketed term becomes zero. Physically, this corresponds to taking measurements at the points on the bearing test fixture where the bearings are attached. No other frequency response function measurements are required for a complete characterization of the bearing stiffness. This is a powerful advantage over static testing techniques. Conventional static testing requires an understanding of the entire test structure so that the deflection of the bearings can be separated from the deflection of the test fixture. The dimension l will be equal to p (the number of bearing connection points) and $p^2/2 + p/2$ FRF measurements will be required (p^2 if symmetry is not invoked).

The next section explores the sensitivity of the bearing stiffness estimation method in the presence of common experimental errors.

4. SENSITIVITY ANALYSIS

The experimental determination of a bearing's stiffness requires accurate experimental measurements of dynamic compliance at the bearing connection points. The accuracy of the stiffness estimate is highly dependent on the sensor locations of the experimental measurements. This result is reasonable because the analysis assumes that the frequency response functions are measured at the exact connection points. This section outlines an analysis performed on a rod vibrating with longitudinal motion to explore the practical limitations of the experimental method to successfully estimate the stiffness of a bearing modification.

The frequency response function of a rod with an attached mass and spring is developed using the classical analytical modal analysis approach. The rod is taken to have one clamped end (at $x = 0$) and a mass and stiffness modification representing a bearing at the opposite end, as shown in Figure 2.

The well known governing differential equation of motion and boundary conditions are readily modified to include the attached mass and spring stiffness:

$$-EA\frac{\partial^2 u}{\partial x^2} + \rho A\frac{\partial^2 u}{\partial t^2} = f(x, t),$$

$$u(0, t) = 0, \qquad EA\frac{\partial u}{\partial x}\bigg|_{x=L} + m\frac{\partial^2 u}{\partial t^2}\bigg|_{x=L} + ku(L, t) = 0. \tag{12}$$

A separation of variables approach is taken to arrive at the analytical solution. Application of the boundary conditions leads to two results: the classical sinusoidal mode shape and a transcendental equation for the roots (modal frequencies) which requires numerical evaluation when m and k are non-zero. The response is measured at x_{out} to a harmonic force applied at x_{in}. This leads to the familiar form of the rod's frequency

response function, complicated somewhat by the addition of the lumped mass and stiffness. A dimensionless FRF can then be written as a function of dimensionless groups:

$$H(\omega)\frac{EA}{L} = \sum_{r=1} \frac{2}{\zeta_1^2(1 - [2\zeta_r]^{-1}\sin 2\zeta_r)} \frac{\sin(\zeta_r x_{in}/L)\sin(\zeta_r x_{out}/L)}{\zeta_r^2/\zeta_1^2 - (\omega^2 L^2\rho/\zeta_1^2 E)}, \tag{13}$$

where the non-dimensional roots (ξ_r) are obtained from the numerical solution of

$$\frac{1}{\zeta_r}\cos\zeta_r + \left(\frac{kL}{EA}\frac{1}{\zeta_r^2} - \frac{m}{\rho AL}\right)\sin\zeta_r = 0.$$

In this analysis the frequency response function is computed twice. In the first case, k and m are set equal to zero to represent the dynamic stiffness of the bearing test fixture without the bearings in place. In the second case, k and m are non-zero and represent the unknown mass and stiffness of the bearing component under test. Using the approach of the previous section, the difference of the inverse of the two FRF's is computed and plotted as a function of the dimensionless frequency. Errors in the experimental test measurement location and sensor calibration may be simulated by using FRF's intentionally computed at locations other than the actual attachment point ($x = L$). Review of the resulting

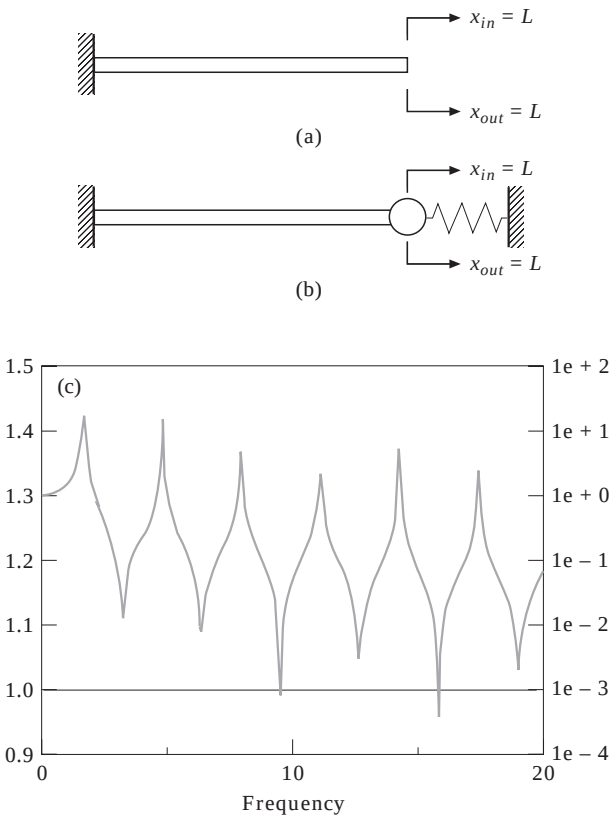

Figure 3. The bearing stiffness estimate obtained with sensors precisely located at the bearing connection point ($x = L$). (a) Physical system before addition of the bearing; (b) physical system with bearing in place; and (c) stiffness estimate (left-hand vertical scale) and drive point FRF (right-hand vertical scale). ——, Stiffness estimate; ....., FRF.

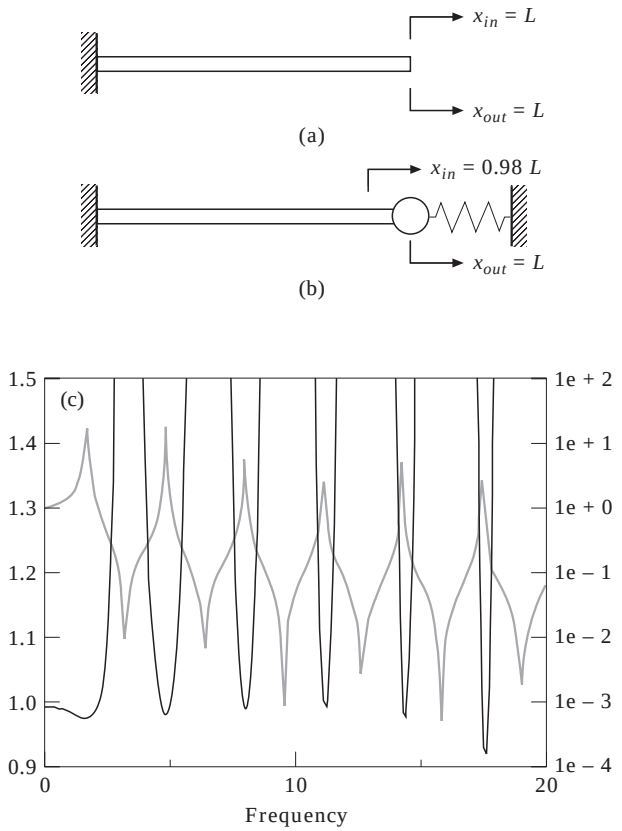

Figure 4. The bearing stiffness estimate obtained with one sensor located off the actual bearing connection point ($x = 0{\cdot}98\ L$). The remaining sensors are precisely located at the connection point. (a) Physical system before addition of the bearing; (b) physical sytem with bearing in place; and (c) stiffness estimate (left-hand vertical scale) and drive point FRF (right-hand vertical scale). Key as Figure 3.

stiffness estimate provides insight into the ability of the experimental technique to correctly calculate the appropriate stiffness of the bearing modification in the presence of realistic experimental errors.

The data shown in Figures 3–5 illustrate the importance of the test measurement location. Each figure shows a different sensor location configuration and the corresponding estimate of the bearing stiffness k as a function of frequency. The drive point frequency response function is also shown for reference.

In Figure 3, the sensors are positioned at the precise location of the spring attachment point ($x = L$). The actual bearing stiffness used to create the FRF's in this simulation is unity, and the stiffness estimate is also one as shown. In Figures 4 and 5 large errors are shown in the stiffness estimate in the presence of sensor positioning errors.

In Figure 4, all of the input and output sensor locations are at the bearing location ($x = L$) except one (either the input or the output sensor). In this case, even slight offsets in sensor location degrade the accuracy of the bearing stiffness estimate as shown in the figure. While the bearing estimate passes near the correct value ($k = 1$) at each modal peak in the reference FRF, the estimate is inaccurate at other frequencies.

Figure 4 highlights the inaccuracies that can arise at frequencies close to the anti-resonances in the FRF's. As seen above, the method requires the inversion of the

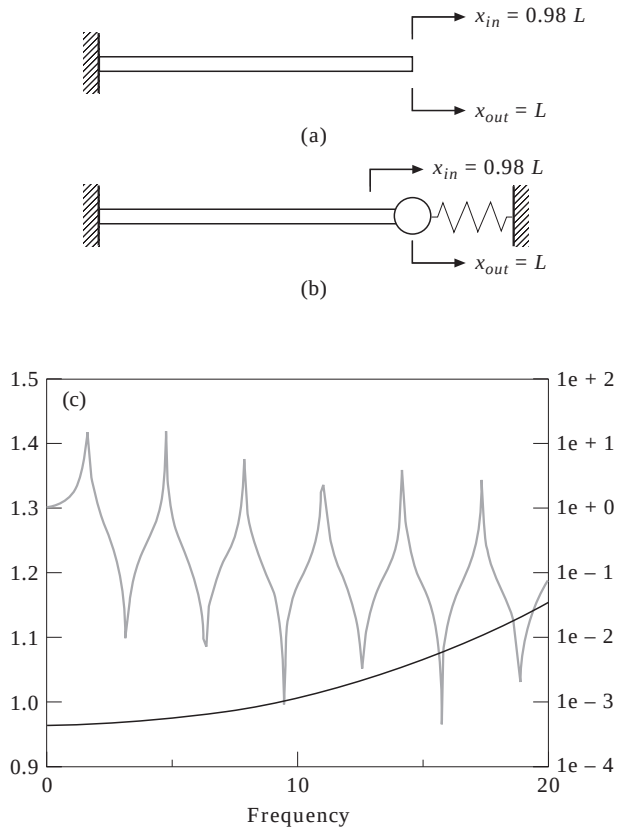

Figure 5. The bearing stiffness estimate obtained by keeping the sensor locations constant before and after connection of the bearing, even if the sensor is not precisely located at the connection point. (a) Physical system before addition of the bearing; (b) physical system with bearing in place; and (c) stiffness estimate (left-hand vertical scale) and drive point FRF (right-hand vertical scale). Key as Figure 3.

frequency response functions. The anti-resonances, which are highly sensitive to noise and experimental error, typically cause substantial error near the FRF zeros. The bearing stiffness estimate is most accurate at the FRF poles.

The stiffness errors that occur when the sensors are offset in pairs are shown in Figure 5. The sensor locations are not at the exact bearing connection location, but are the same for the FRF measurements taken before and after installation of the bearing. In this case, the stiffness estimation algorithm is much less sensitive to the offset and reasonable offsets can be tolerated without substantial degradation in accuracy.

A reasonable stiffness estimate may be obtained even with sensors located off the precise bearing connection point provided that the sensor locations remain constant throughout the experimental testing.

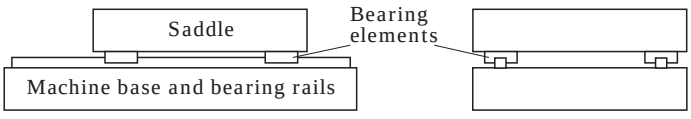

Figure 6. The test hardware used in the experimental measurement of the bearing stiffness.

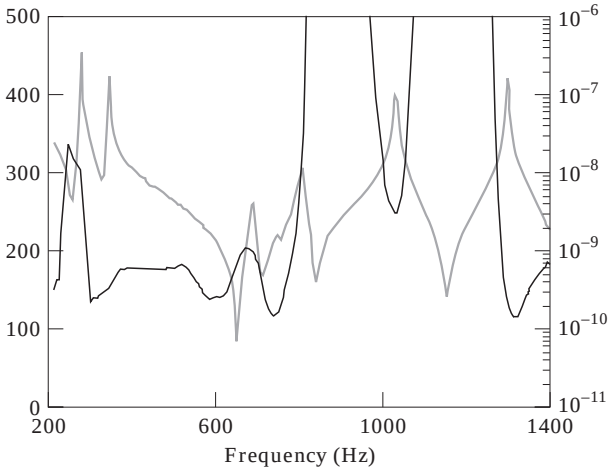

Figure 7. An estimate of the spring stiffness in a precision bearing system. —, Bearing stiffness estimate; ·····, drive point FRF.

5. EXPERIMENTAL VERIFICATION OF STIFFNESS METHOD: PRECISION ROLLING ELEMENT BEARINGS

The bearing stiffness estimation algorithm was applied to the rolling element bearing of a precision machine tool slideway. The slideway, which is shown in Figure 6, is composed of four recirculating ball bearing elements, two of which were removed during testing to reduce the number of measurements required. The test fixture weighs 1000 N and is made of two steel plates, two bearing rails and bearing elements. The bearing manufacturer states that the bearings under test offer a static stiffness of 220 N/micron. Although these quoted stiffness values are obtained by various techniques, in general, they serve as useful estimate of the actual performance.

The bearings under test may be removed from the bearing rails by sliding the saddle off the table. As a result, the mass of the system is unchanged between the two test conditions: connected and unconnected. A total of 16 FRF measurements were taken with the bearings connecting the saddle and the table. Eight additional measurements were taken after the saddle was removed from the table. Using the algorithm outlined above, a frequency dependent estimate of the bearings' stiffness was calculated, as shown in Figure 7. The figure suggests that in the frequency range of 200–800 Hz, the stiffness estimate centres near 180 N/micron. This correlates fairly well with the manufacturer's claimed stiffness of 220 N/micron.

The two frequency ranges in which the stiffness estimate is poor (800–1000 Hz and 1100–1300 Hz) centre around two zeros in the frequency response function measurements taken without the bearings. As seen before, these zeros lead to large errors in the stiffness estimate. At other frequencies, the estimate is quite good.

As a final check of the stiffness estimation algorithm, the experimentally determined stiffness of 180 N/micron is now used to synthesize the frequency response functions of the fully assembled test fixture. The frequency response functions of the total test fixture are synthesized using only the FRF's of the individual components (as measured experimentally) and the static stiffness estimate of the bearings (as provided by the proposed method). The synthesized FRF shown in Figure 8 is constructed using the stiffness estimate of 180 N/micron and an FRF of the test fixture without the bearing ($\mathbf{H}_0$). The actual frequency response function of the test fixture with bearing ($\mathbf{H}$) is shown for comparison.

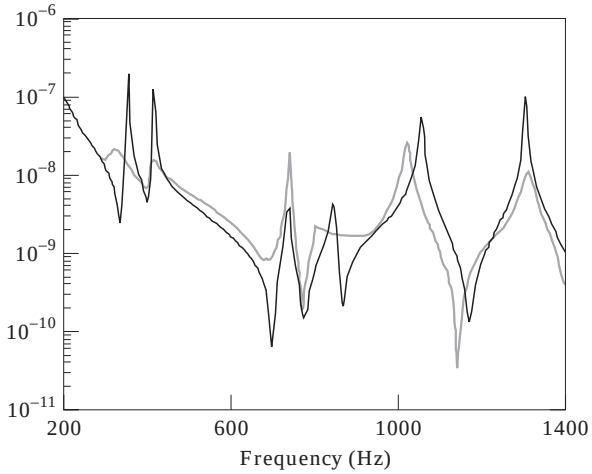

Figure 8. The synthesized FRF as calculated from the experimental stiffness estimate. ——, Measured frequency response function; ·····, synthesized frequency response function.

The results of Figure 8 are encouraging, given the physical difficulty of predicting the total response from the individual components. A typical drive point frequency response function of the unassembled test fixture undergoes a substantial change when the test fixture is assembled with the addition of the bearings to the system. In this example, the unconnected test fixture has only two poles in the frequency range of 0–1400 Hz. The connected test fixture has the six poles shown in Figure 8. The synthesized FRF, which is calculated using the drive point FRF of the unconnected system and the bearing stiffness estimate, compares reasonably well with the actual connected frequency response measured at the same location on the test fixture.

6. CONCLUSIONS

The proposed experimental method of estimating the stiffness of precision bearings has been shown to provide reasonable estimates of bearing components. An analysis of the method's sensitivity to errors in sensor location has demonstrated several practical advantages of the method over traditional static testing.

(1) A complete characterization of the test fixture is unnecessary. Instead, frequency response function measurements are required at only the bearing connection locations.

(2) The stiffness estimate properly separates the test fixture compliance from the bearing compliance.

(3) Considerations such as the boundary conditions of the test fixture do not affect the results, provided that they remain constant during the testing. Free boundaries are a convenient choice and may be adequately simulated using a soft suspension of the test fixture.

The sensitivity analysis presented in this paper highlights important issues that can degrade the accuracy of the proposed method.

(1) Sensor locations must be kept constant throughout testing to ensure accurate results. In practice, dedicated sensors used to gather the response may be left attached to the test fixture to maintain the location.

(2) The mass of the bearing components is typically known and may be used to improve the accuracy of the stiffness estimate straightforwardly. A correction term of $-\omega^2\mathbf{M}$ may be applied to the frequency dependent stiffness estimate to make this allowance. At low frequencies, the magnitude of the correction is small with respect to the other terms present in the impedance matrices.

(3) Similarly, the damping in the bearing components, which may be significant, can be either corrected for in the stiffness estimate, or extracted from the results assuming a hysteretic or other damping model.

ACKNOWLEDGMENT

The authors wish to thank Mr Byron Knapp for his experimental testing of the bearings and test fixtures.

REFERENCES

1. B. J. Stone 1982 *Annals of CIRP* **31**, 529–538. The state of the art in the measurement of the stiffness and damping of rolling element bearings.
2. T. L. H. Walford and B. J. Stone 1980 *Journal of Mechanical Engineering Science*, 22–4. The measurement of the radial stiffness of rolling element bearings under oscillating conditions.
3. T. L. H. Walford and B. J. Stone 1980 *Proceedings of the 2nd International Conference on Vibrations in Rotating Machinery*. Some stiffness and damping characteristics of angular contact bearings under oscillating conditions.
4. J. Kraus, J. J. Blech and S. G. Braun 1987 *Journal of Vibration, Acoustics, Stress, and Reliability in Design* **109**, 235–240. *In situ* determination of rolling bearing stiffness and damping by modal analysis.
5. R. Tiwari and N. S. Vyas 1995 *Journal of Sound and Vibration* **187**, 229–239. Estimation of non-linear stiffness parameters of rolling element bearings from random response of rotor–bearing system.
6. H. G. Lee and B. J. Dobson 1991 *Journal of Sound and Vibration* **145**, 61–81. The direct measurement of structural mass, stiffness, and damping properties.
7. B. J. Dobson 1991 *Proceedings of the International Modal Analysis Conference*, 555–562. Comparing measured and predicted spatial properties.